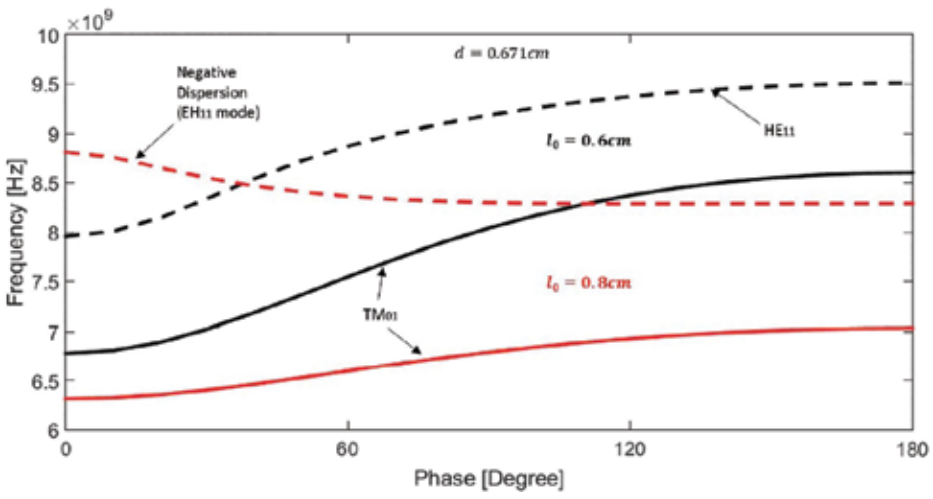

Figure 7. Dispersion diagram for the lowest order modes with different corrugation depths in a cylindrical SWS (solid lines represent the first mode while dashed lines represent the second mode for each corrugation depth indicated) with mean radius R_0=1.6 cm and period d=0.671 cm.

For the sinusoidal SWS with period cm the hybrid EH11 mode (its structure is shown in Fig. 8) displays negative dispersion when the corrugation depth mm (Fig. 7).

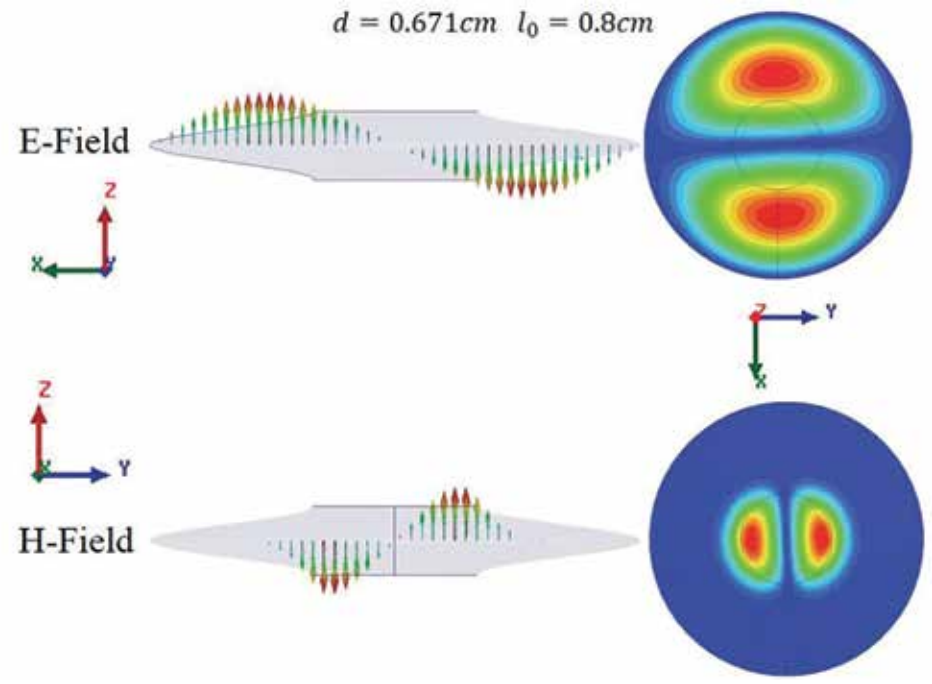

Figure 8. Structure of the hybrid EH11 mode in an all-metallic SWS with sinusoidal corrugation.

Thus, we have shown that the well-known properties of MSWSs are, in fact, common properties of all-metallic periodic systems with deep corrugations.

It is conceivable that additional properties of MSWSs will be identified in the future that will not have similar properties in traditional SWSs.

IV.CONCLUSIONS

Using the metamaterial concept, we designed a novel effective microwave oscillator with a MSWS and have achieved record high output power of about 100 MW in experiment, which agrees with PIC simulation results for the reduced input parameters. Computer simulations show that with applied voltage 400 kV, radiation power is 260 MW with frequency 1.4 GHz. An efficiency of 15% is achieved with very fast rise time 4 ns. The designed MSWS consisting of rings with oppositely oriented cuts with small period that is much less than wavelength shows metamaterial properties such as below cut-off propagation, and negative dispersion.

We also show that long before the appearance of the concept of MSWSs, many researchers in vacuum electronics worked with SWSs having properties similar to the known (at present) "unique" properties of MSWSs without knowing about it.

ACKNOWLEDGEMENTS

This research was supported by AFOSR MURI Grant FA9550-12-1-0489. The author would like to thank Sarita Prasad, Kevin Shipman, Dmitrii Andreev, Daniel Reass, Mikhail Fuks, and Edl Schamiloglu for their assistance and for useful discussions.

REFERENCES

1. V.G. Veselago, "The Electrodynamics of Substances with Simultaneously Negative Values of e and u" Sov. Phys. Usp., vol. 10, pp. 509-514 (1968).

2. J.B. Pendry, A.J. Holden, D.J. Robbins, and W.J. Steward, "Magnetism from Conductors and Enhanced Nonlinear Phenomena," IEEE Trans. Microw. Theory Techn., vol. 47, pp. 2075-2084 (1999).

3. D.R. Smith, W.J. Padilla, D.C. Vier, S.C. Nemat-Nasser, and S. Shultz, "Composite Medium with Simultaneously Negative Permeability and Permittivity," Phys. Rev. Lett., vol. 84, pp. 4184-4187 (2000).

4. R. Marques, F. Martin, and M. Sorolla, *Metamaterials with Negative Parameters: Theory, Design, and Microwave Applications* (John Wiley and Sons, Inc., New York, NY, 2008).

5. F. Capolino, Ed., Theory and Phoenomena of Metamaterials (CRC Press, Boca Raton, FL, 2009).

6. J.B. Pendry, D. Schuring, and D.R. Smith, "Controlling Electromagnetic Waves," Science, vol. 312, pp. 1780-1782 (2006).

7. Schamiloglu, E., "Dispersion Engineering for High Power Microwave Amplifiers," Proceedings of the 2012 EAPPC-Beams (Karlsruhe, Germany, September 2012).

8. J.S. Hummelt, S.M. Lewis, M.A. Shapiro, and R.J. Tempkin, "Design of a Metamaterial-Based Backward-Wave Oscillator," *IEEE Trans. Plasma Sci.*, vol. 42, pp. 930-936 (2014).

9. S. C. Yurt, M. I. Fuks, S. Prasad and E. Schamiloglu, "Design of a Metamaterial Slow Wave Structure for an O-Type High Power Microwave Generator," *Phys. Plasmas*, vol. 23, no. 12, pp. 123115-1-7, 2016.

10. S.C. Yurt, S. Prasad, K. Ilyenko, M. Fuks, and E. Schamiloglu, "Modeling Dispersion Diagram for Metamaterial-like Slow Wave Structure" Proceedings IVEC'14 (Monterey, CA, April 2014).

11. S.C. Yurt, S. Prasad, K. Ilyenko, M. Fuks, and E. Schamiloglu, "O-Type Oscillator with Metamaterial-like Slow-Wave Structure" Proceedings IVEC'14 (Monterey, CA, April 2014).

12. S.C. Yurt, A. Elfrgani, M. Fuks, K. Ilyenko, and E. Schamiloglu, "Similarity of Properties of Metamaterial Slow Wave Structures and Metallic Periodic Structure," *IEEE Trans. Plasma Sci.*, vol.44, pp. 1280-1286 (2016).

13. B. Goplen, L. Ludeking, D. Smith and G. Warren, "User-Configurable MAGIC for Electromagnetic PIC Simulations," *Comput. Phys. Commun.*, vol. 87, pp. 54-87, 1995.

14. [Online]. Available: http://www.cst.com/. [Accessed 10 October 2016].

15. [Online]. Available: http://www.ansys.com/products/Electronics/ANSYS-HFSS. [Accessed 10 October 2016].

16. J. Lu, T. M. Grzegorczyk, Y. Zhang, J. Pacheco, B. I. Wu, J. A. Kong and M. Chen, "Cerenkov Radiation in Materials with Negative Permittivity and Permeability," *Optics Express*, vol. 11, p. 723–734, 2003.

17. D. M. French, D. Shiffler and K. Cartwright, "Electron Beam Coupling to a Metamaterial Structure," *Phys. Plasmas*, vol. 20, pp. 083116-1-8, 2013.

18. M. I. Fuks, E. Schamiloglu and Y. D. Li, "RF Priming for Operation of Relativistic TWT with Reflections Near Cyclotron Resonance," *IEEE Trans. Plasma Sci.*, vol. 42, no. 1, pp. 38-41, 2014.

Sabahattin Yurt can be reached by E-mail at cyurt@unm.edu.

Improving PET Quantitation with Denoising, Motion Compensation, and Deblurring

Joyita Dutta
IEEE Member, Author

Positron emission tomography (PET) enables 3D visualization of vital physiological information, e.g., metabolism, blood flow, and neuroreceptor concentration by using targeted radioisotope-labeled tracers. Quantitative interpretation of PET images is crucial both in diagnostic and therapeutic contexts. As a result of its unique functional capabilities, PET imaging plays a pivotal role in diagnostics and in therapeutic assessment in many areas of medicine, including oncology, neurology, and cardiology. Accurate quantitation requires correction of PET raw data and/or images for a number of physical effects. These include attenuation correction, randoms and scatter correction, subject motion correction, and partial volume correction. We have developed a range of techniques that address the PET denoising, motion compensation, deblurring problems. Several of these methods greatly enhance the quantitative capabilities of PET particularly by incorporating information from an anatomical imaging modality such as magnetic resonance imaging (MRI).

IMAGE DENOISING

Faced with a fundamental tradeoff between radiation dose and image noise, PET data is inherently noisy. The high levels of noise in PET images pose a challenge to accurate quantitation. This issue is particularly well-pronounced at the early time frames of dynamic PET images, which are usually short to capture rapid changes in tracer uptake patterns. In order to improve image quality and quantitative accuracy, statistical image reconstruction algorithms model the Poisson characteristics of PET data and employ numerical optimization algorithms to solve the corresponding optimization problem [1, 2]. Common reconstruction procedures, such as ordered subsets expectation maximization, are therefore routinely followed by a post-filtering step for denoising the reconstructed image. A range of strategies have been proposed for post-reconstruction denoising of both static and dynamic PET images [3, 4]. In recent years, image denoising based on non-local means (NLM) has become popular [5]. Unlike conventional neighborhood filters, which use local similarities, in this technique, the search for voxels similar to a given voxel is no longer restricted to its immediate vicinity. This is an attractive feature for dynamic PET images since tissue types exhibiting similar tracer

ARTICLES Continued on **PAGE 14**

PET Quantitation Continued from **PAGE 13**

dynamics are often distributed all over the body. We have developed denoising techniques for dynamic PET images which are inspired by NLM denoising.

NLM denoising computes weighted averages of voxel intensities assigning larger weights to voxels that are similar to a given voxel in terms of their local neighborhoods or patches. In our work [6], we introduced three key modifications to tailor the original NLM framework to dynamic PET. Firstly, we derived similarities from less noisy later time points to denoise the entire time series. Secondly, we used spatiotemporal patches for robust similarity computation. Finally, we used a spatially varying smoothing parameter based on a local variance approximation over each spatiotemporal patch. To assess the performance of our denoising technique, we performed realistic simulations on a dynamic digital phantom based on the Digimouse atlas. For experimental validation, we denoised [18F]FDG PET images from a mouse study and a hepatocellular carcinoma patient study. We compared the performance of NLM denoising with four other denoising approaches – Gaussian filtering, PCA, HYPR, and conventional NLM based on spatial patches. The simulation study revealed noticeable improvement in bias-variance performance achieved
using our NLM technique relative to all the other methods. The experimental data analysis revealed that our technique leads to clear improvement in contrast-to-noise ratio in Patlak parametric images generated from denoised preclinical and clinical dynamic images, indicating its ability to preserve image contrast and high-intensity details while lowering the background noise variance. In a follow-up study, we extended the denoising framework by using non-local Euclidean means [7]. To further improve denoising performance along sharp edges, we used anatomical guidance to limit the spatial window for non-local similarity computation. We tested this anatomically guided denoising technique by performing simulations on the BrainWeb digital phantom and on human datasets (Fig. I A-C) and demonstrated its robustness particularly at high noise levels and its ability to preserve sharp edges (e.g. tissue and organ boundaries).

MOTION COMPENSATED IMAGE RECONSTRUCTION

Pulmonary PET imaging is confounded by blurring artifacts caused by respiratory motion, which degrade both image quality and quantitative accuracy. Simultaneous whole body PET/MRI is an emerging technology that combines the strengths of two complementary imaging modalities and is becoming an increasingly potent tool for integrated imaging. While PET reveals only functional or physiological information, MRI is able to generate structural or anatomical information, generally with higher resolution. In the context of lung imaging, where PET scans are severely compromised by respiratory motion, we have developed a maximum a posteriori estimation framework that incorporates deformation fields derived from simultaneously acquired MRI data.

We developed and implemented a complete data acquisition and processing framework for respiratory motion compensated image reconstruction using simultaneous PET/MRI and validated it through simulation and clinical patient studies [8, 9]. For fast acquisition of high-quality 4D MR images, we developed a novel Golden-angle RAdial Navigated Gradient Echo (GRANGE) pulse sequence and used it in conjunction with sparsity-enforcing k-t FOCUSS reconstruction. We used a 1D slice-projection navigator signal encapsulated within this pulse sequence along with a histogram-based gate assignment technique to retrospectively sort the MR and PET data into individual gates. We computed deformation fields for each gate via nonrigid registration. The deformation fields are incorporated into the PET data model as well as utilized for generating dynamic attenuation maps. The framework was validated using simulation studies on the 4D XCAT phantom and three clinical patient studies that were performed on the Biograph mMR, a simultaneous PET/MR scanner. We compared motion corrected results with ungated and single-gate reconstruction results and demonstrated that this method led to robust increases in contrast-to-noise ratio of high-intensity features of interest affected by respiratory motion (Fig. II A-C). This technique enables the generation of PET images free of motion artifacts, which leads to improved image quantitation, thereby facilitating lung cancer staging and treatment optimization.

PARTIAL VOLUME CORRECTION

The quantitative accuracy of PET is degraded by partial volume effects caused by the limited spatial resolution capabilities of PET scanners. We developed an image deblurring technique that uses the spatially varying point spread function of the scanner measured in the image space. To stabilize the deconvolution problem, we introduce the joint entropy between the PET image and a high-resolution MR image as an information theoretic penalty function [10]. We implemented a computationally efficient framework for solving the corresponding numerical optimization problem. By means of simulations on the BrainWeb phantom, we showed that our method leads to faster convergence and a lower mean squared error. The technique was applied to Hoffman brain phantom data as well as human data. Compared to standalone deblurring, which tends to amplify noise, the joint entropy prior leads to a smooth PET image with sharp boundaries consistent with MRI. One challenge with our approach, however, is the spurious interpretation of intermediate intensity values that are generated by the blurring effects as separate peaks in the joint probability density function. We further extended this method to include a spatial encoding scheme that leads to a weighted joint entropy regularizer which suppresses the effect of the spurious peaks [11]. Our studies on the BrainWeb digital phantom and the Hoffman experimental phantom show that the resultant technique reduces mean squared error in the deblurred PET image and leads to a more realistic gray-to-white contrast ratio. We also showed that the spatially encoded joint entropy prior is more robust than ordinary joint entropy in the presence of structural discrepancies between the PET and the anatomical images and suppresses artifacts arising from such discrepancies. The method was applied to range of human studies (Fig. III A-C).

PET Imaging of tau tangles in the brain is very promising for monitoring the progression of Alzheimer's disease and chronic traumatic encephalopathies. However, partial volume effects associated with the limited PET spatial resolution pose a challenge to quantitation. Application of our anatomically guided deblurring method to a pool of clinical subjects revealed a marked improvement in the correlation of PET measures with well-recognized clinical metrics of cognitive performance [12].

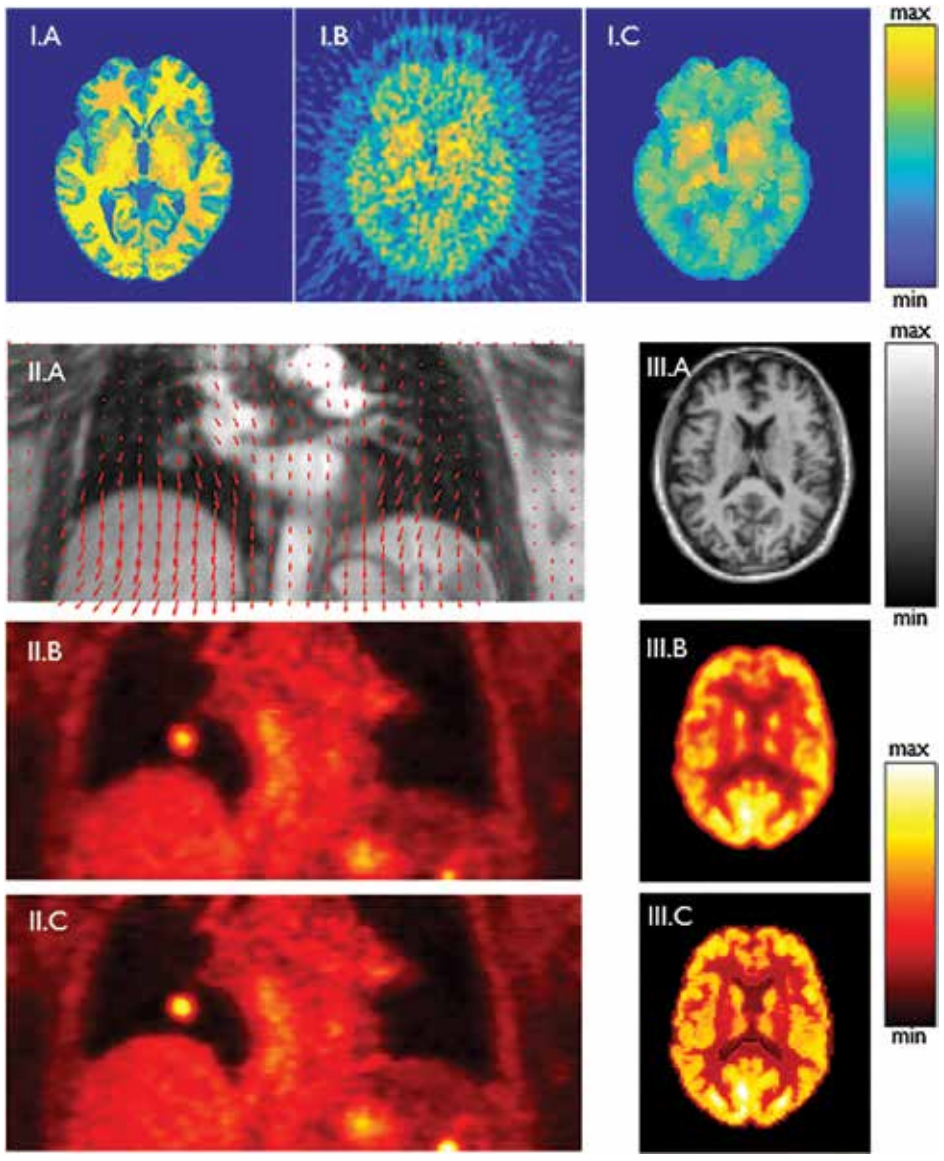

I. Anatomically guided nonlocal means denoising: A. Segmented MR B. Noisy frame from dynamic [18]F AV1451 image of neurofibrillary tangles in a human subject with mild cognitive impairment. C Denoised PET image. II. Motion compensation using simultaneous PET/MR: A. MR image with superimposed displacement fields. B. Uncorrected PET image showing a lung lesion with motion induced blurring. C. Motion corrected PET image. III. Anatomically guided image deblurring: A. TI weighted MR image of a human subject. B. [18]F FDG PET image. C. Deblurred PET image based on anatomical prior information.

REFERENCES

1. Leahy RM, Qi J (2000) Statistical approaches in quantitative positron emission tomography. *Stat Comput* 10: 147-165.

2. Dutta J, Ahn S, Li Q (2013) Quantitative statistical methods for image quality assessment. *Theranostics* 3(10):741-56.

3. Kimura Y, Senda M, Alpert N (2002) Fast formation of statistically reliable FDG parametric images based on clustering and principal components. *Phys Med Biol* 47: 455–468

4. Christian BT, Vandehey NT, Floberg JM, Mistretta CA (2010) Dynamic PET denoising with HYPR processing. *J Nucl Med* 51: 1147–1154.

5. Buades A, Coll B, Morel JM (2005) A non-local algorithm for image denoising. In: *Proc IEEE Comput Soc Conf Comput Vis Pattern Recognit*. volume 2, pp. 60–65.

6. Dutta J, Leahy RM, Li Q. Non-local means denoising of dynamic PET images. *PLOS One*. 2013 Dec 5;8(12):e81390.

7. Dutta J, El Fakhri G, Li Q (2016) PET image denoising using anatomically guided non-local Euclidean medians. *IEEE Nuclear Science Symposium and Medical Imaging Conference*, Strasbourg, France, Oct 29–Nov 6, 2016.

8. Dutta J, El Fakhri G, Huang C, Petibon Y, Reese TG, Li Q (2013) Respiratory motion compensation in simultaneous PET/MR using a maximum *a posteriori* approach. In: Proc IEEE International Symposium on Biomedical Imaging, pp. 800–803.

9. Dutta J, Huang C, Li Q, El Fakhri G (2015) Pulmonary imaging using respiratory motion compensated simultaneous PET/MR. *Med Phys* 42(7):4227-40.

10. Dutta J, El Fakhri G, Zhu X, Li Q (2015) PET point spread function modeling and image deblurring using a PET/MRI joint entropy prior. In: *Proc IEEE International Symposium Biomedical Imaging*, New York, NY, Apr 16–19, 2015, pp. 1423–1426.

11. Dutta J, El Fakhri G, Li Q (2015) Spatially encoded joint entropy prior for PET image deblurring. *IEEE Nuclear Science Symposium and Medical Imaging Conference*, San Diego, CA, Oct 31–Nov 7, 2015.

12. Dutta J, Li Q, Johnson K, Zhu X, El Fakhri G (2014) High resolution PET imaging of tau using an MR-based information theoretic anatomical prior. *J Nucl Med* 55 (supplement 1): 642-642.

Joyita Dutta can be reached by E-mail at Joyita_Dutta@uml.edu.

NOT MIND OVER MATTER

Be who you are and say what you feel because those who mind don't matter and those who matter don't mind.

Theodor Seuss Geisel

IS EVERYBODY...

Happy people don't need to have fun.

Jean Stafford